



Adsorption of Reactive Blue19 from Aqueous Environment on Magnesiumoxide Nanoparticles: Kinetic, Isotherm and Thermodynamic Studies

Chinenye Adaobi Igwegbe^{1*}, Artur Marek Banach², Shahin Ahmadi³

¹Department of Chemical Engineering, Nnamdi Azikiwe University, Awka, Nigeria

²Department of Biochemistry and Environmental Chemistry, Institute of Biotechnology, The John Paul II Catholic University of Lublin, Lublin, Poland

³Department of Environmental Health, School of Public Health, Zabol University of Medical Sciences, Zabol, Islamic Republic of Iran

Abstract Water pollution due to discharge of dye containing effluents is one of the environmental problems of serious concern today. The main purpose of study is to investigate the efficiency of magnesium oxide nanoparticles (MgO-NPs) on the removal of Reactive blue 19(RB19) from its aqueous solution. The influence of various process parameters such as pH (3 – 11), dosage of MgO-NPs (0.3 – 2.3 g/L), contact time (20 – 150 min), and concentration of RB19 (50 – 200mg/L) was studied using batch adsorption technique. Thermodynamic parameters were also evaluated. The maximum RB19 removal efficiency of 81% was reached at an optimum contact time of 60 min, pH 3, MgO NPs dosage of 1.5 g/L, and initial RB19 concentration. RB19 adsorption on MgO NPs was found to depend on the pseudo-second-order kinetic model which indicates a chemisorption process. The Freundlich adsorption isotherm model best described the removal of RB19 on MgO NPs. The adsorption process was found to be favourable since the intensity of adsorption, n (0.35) lies within 1 to 10. The maximum monolayer adsorption capacity, q_m of 7.9 mg/g was obtained. The RB14 adsorption was also found to endothermic in nature. The efficiency was decreased with an increase in temperature implying the process should be performed at a controlled temperature. Results obtained showed that the MgO-NPs could effectively remove RB19 from the RB19 containing effluent.

Keyword: Adsorption Isotherm, Kinetics, Nanoparticles, Reactive blue 19, Thermodynamics

1. Introduction

The use of the different kinds of the colors and chemical materials in dyeing processes causes significant creation in wastewater features of industries such as the difference in color, pH and chemical materials [1]. The discharge of colored wastewater into the environment and aquatic ecosystem prevents the penetration of light into the water depth [2, 3]. This can also cause a disturbance in the process of photosynthesis and destruction of the aquatic plants [3]. Besides, most of the consumable dyes used by the textile industries have an organic origin and have been mostly made from diazo, phthalocyanine and anthraquinone salts that have benzene loop that can be toxic and carcinogenic in nature [4, 5]. Reactive dyes are one of the most common dyes consumed in textile industries after azo colors group [6]. Reactive blue 19 (RB19) also known as Remazol Brilliant blue is an anthraquinone dye used by the textile industries [1, 7]. Therefore, the removal of the dye from wastewaters is necessary.



Researchers have proposed several treatment methods for the removal of dyes from contaminated waters which include flocculation [8], coagulation [9], adsorption [10, 11, 12], advanced oxidation process [13] and fungal decolorisation [14, 15] and other processes. The adsorption process is the most preferred and widely applied method in industries for eliminating organic compounds [11]. Also, in adsorption, the production of harmful byproducts do not occur [9]. The most commonly used adsorbing materials are the activated carbons but cannot be easily regenerated [16, 11]. Nanoparticles (NPs) are referred to particles with a diameter of less than 100 nm [17]. Today NPs are widely used in different industries such as textile, polishing paint and oil, and diagnosis of diseases [18]. So research on nanotechnology and its development have also been increased extremely. Its potential is as a result of its unique physicochemical properties in nanoscale [17]. Magnesium oxidenanoparticles (MgO NPs) are basic oxides group and have provided a wide range of application in adsorption process [19]. The most important characteristics of MgO NPs are availability, low cost, non-volatility, non-toxicity, stability, reusability, adsorption capacity and high reactivity [20]. MgO NPs are widely used as a catalyst, treatment of hazardous materials and resistant materials [21].

The main purpose of the study is to investigate the efficiency of MgO NPs on the removal of RB19 from its aqueous solution. The influence of various factors such as the contact time, MgO NPs dosage, initial pH and initial concentration of RB19 were studied, and their optimum conditions were also determined to enhance the RB19 adsorption efficiency. The isotherm, kinetic and thermodynamics of the adsorption process were also studied.

2. Materials and Methods

2.1. Materials

All the chemicals used in the present study were of analytical grade and were procured from Sigma-Aldrich Co, Germany. The MgO nanoparticles (MgO NPs) with 98% purity and particle size of 50 nm were purchased from Sigma-Aldrich and were used without any further treatment. In this study, RB19 (chemical formula: $C_{22}H_{16}N_2Na_2O_{11}S_3$ and molecular weight: 626.54 g/mol), an anionic dye was used as the pollutant. The chemical structure of RB19 is shown in Figure 1.

2.2. Instrumental characterization of the adsorbent (MgO NPs)

Scanning electron microscopy (SEM) was used to determine the surface morphology of MgO NPs via a SEM machine (HITACHI Model S-3000H). The X-ray diffraction was done using an XRD machine (SMART Lab) to determine the crystalline property and diffraction pattern of the adsorbent.

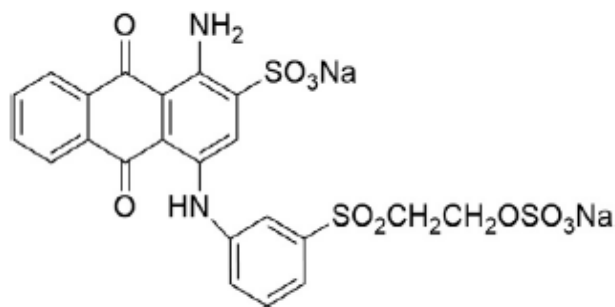


Figure 1: The structure of RB19 dye

2.3. Point zero charge of the MgO NPs

One of the most important features of an adsorbent is the point zero charge, pH_{ZPC} . The point where the charge on catalyst surface is zero is the point of zero charge [22]. The pH_{ZPC} of the MgO NPs was determined according to the method described by [22]. To determine the pH_{ZPC} , 50 ml of potassium nitrite (0.01M) was added to Erlenmeyer flasks and the pH was adjusted in the range of 2 to 14 and NaOH. Then, 0.2g of NPs was added and mixed in a



shaker at 180 rpm for 24 h. After the stirring, the final pH was measured using a MIT65 pH meter. The intersection point of the curve (change of pH versus initial pH) was recorded as pH

2.4. Batch Adsorption Studies

A stock solution of RB19 was prepared by dissolving a known mass of dye in 1L of doubled distilled water where other concentrations (50, 90, 100, 120, 150, 180, 200 mg/L) for the study can be prepared by dilution. The pH, MgO NPs dosage, initial dye concentration, contact time and solution temperature were varied to study their effects on the adsorption of RB19 on MgO NPs. Batch adsorption experiments were carried out by using 250 mL Erlenmeyer flask. For each adsorption test, 100mL of the dye solution with a certain concentration was added into the Erlenmeyer flask and a certain dosage of adsorbent was added to the flask and then mixed with the magnetic stirrer (MODEL: MSH basic) at 180 rpm for a specified time. The initial and final RB19 concentrations remaining in solutions were analyzed by a UV-visible recording spectrophotometer (Shimadzu Model: LUV-100A), Construction Japan and were determined at a wavelength of maximum absorbance, $\lambda_{\max} = 595$ nm. The removal efficiency, R (%) and the amount of RB14 adsorbed, q_e (mg/g) of the studied parameters were calculated based on the following formulas [23, 24]:

$$\%R = \frac{(C_0 - C_f)}{C_0} 100 \quad (1)$$

$$q_e = \frac{(C_0 - C_e)V}{M} \quad (2)$$

Where C_0 and C_f is the initial and final RB19 concentration, respectively, C_e is the final equilibrium liquid phase concentration of RB19 (mg/g), M is the mass of adsorbent (g) and V is the volume of the RB19 solution (L).

2.5. Adsorption Kinetics

Kinetic models are used to examine the rate of the adsorption process and the potential rate controlling step

The pseudo-first-order rate equation is expressed as [23]:

$$\text{Log}(q_e - q_t) = \text{Log}(q_e) - \frac{k_1}{2.303} t \quad (3)$$

Where q_e and q_t are the amounts of RB14 adsorbed (mg/g) at equilibrium and time t (min), respectively, and k_1 is the rate constant of adsorption (min^{-1}). Values of k_1 were calculated from the slope of plots of $\log(q_e - q_t)$ against (t) at different concentrations.

The pseudo-second-order rate equation is given as [25]:

$$\frac{t}{q_t} = \frac{1}{k_2 q_e^2} + \frac{t}{q_e} \quad (4)$$

Where k_2 is the second order rate constant ($\text{g mg}^{-1} \text{min}^{-1}$), q_t and q_e are the amounts of RB19 adsorbed on the adsorbent (mg/g) at equilibrium and at time t respectively.

2.6. Adsorption Isotherm

There are many isotherm models for experimental data analysis and description of equilibrium in adsorption such as Langmuir, Freundlich, and Tempkin. The Langmuir isotherm is based on single layer and homogenous adsorbed material with the same energy on the surface. The Langmuir isotherm model is presented as [26]:



$$\frac{C_e}{q_e} = \frac{1}{q_m} + \frac{1}{q_m K_L} \quad (5)$$

Where q_m is the maximum adsorption capacity (mg/g), q_e is the amount of adsorbate adsorbed on adsorbent (mg/g), K_L is the Langmuir isotherm constant related to the affinity of the binding sites and energy of adsorption (L/mg). The essential specifications of a Langmuir isotherm can be expressed in the idiom of a dimensionless constant separation factor or equilibrium parameter, R_L which is defined as [10, 25, 27]:

$$R_L = \frac{1}{1 + K_L C_0} \quad (6)$$

The R_L values indicates whether the isotherm is either favorable ($0 < R_L < 1$), unfavorable ($R_L > 1$), linear ($R_L = 1$) or reversible ($R_L = 0$) [10, 28].

Freundlich isotherm was calculated using a heterogeneous surface with non-uniform distribution of surface adsorption heat. The Freundlich isotherm is given by [25, 26]:

$$\text{Log} q_e = \frac{1}{n} \text{Log} C_e + \text{Log} k_f \quad (7)$$

Where q_e is the amount of RB19 adsorbed (mg/g), C_e is the equilibrium concentration of RB19 in solution (mg/L), and K_f and n are the constants incorporating the factors affecting the adsorption capacity and intensity of adsorption, respectively.

With regards to possible interactions between adsorbent and adsorbate species, the adsorption theory is corrected. The heat of adsorption of all molecules in the adsorption layer is linearly reduced by the amount of coating. The Tempkin isotherm has been expressed by the following equation [29]:

$$q_e = B_1 \text{Ln}(A_T) + B_1 \text{Ln}(C_e) \quad (8)$$

A plot of q_e versus $\text{Ln} C_e$ enables the determination of the constants A_T and B_T . B_T is the heat of sorption and A_T is the equilibrium binding constant.

2.7. Thermodynamics Study

The three basic parameters for thermodynamic study are the standard enthalpy (ΔH^0), Gibbs free energy (ΔG^0) and standard entropy (ΔS^0). The free energy change can be determined by the following relation [26, 30]:

$$\Delta G^0 = -RT \ln K \quad (9)$$

Where K is the equilibrium constant, T is the temperature in (K), R is the universal gas constant. The free energy change can be expressed in terms of enthalpy change of sorption as a function of temperature as follows [29, 30]:

$$\Delta G^0 = \Delta H^0 - T\Delta S^0 \quad (10)$$

Where R is the universal gas constant ($8.314 \text{ J mol}^{-1}\text{K}^{-1}$), T is the temperature (K) and K is the distribution coefficient. The ΔH^0 and ΔS^0 values were derived from the linear plot of $\text{Ln} K$ against $1/T$, which are the slope and intercept of the graph linear equations, respectively. The sorption behaviors of different RB19 concentrations onto MgO NPs were critically investigated at 293, 313, and 308 K. Thermodynamic parameters were calculated from following equations 11 and 12 [30]:

$$\text{Ln} k_c = \frac{\Delta S^0}{R} - \frac{\Delta H^0}{RT} \quad (11)$$

$$K_c = \frac{q_e}{C_e} \quad (12)$$

Where C_e is the equilibrium concentration of RB19 and q_e is the amount of RB19 adsorbed per unit weight of MgO NPs at equilibrium concentration (mg/g).



3. Results and Discussion

3.1. Characterization of the MgO nanoparticle

The specific surface area is one of the parameters determining the adsorption capability of an adsorbent substance and when the specific surface area of the adsorbent substance is high, the adsorbent will have more pores leading to higher level of contact with the adsorbate [31]. As it is clear in the SEM picture (Fig. 2), the prepared adsorbent has a very high porosity for trapping the dye pollutant on its surface. The XRD image showed that the maximum peak is around 43° with exceedingly high intensity. The presence of broad peaks on the XRD image proves the crystalline nature of MgO NPs,

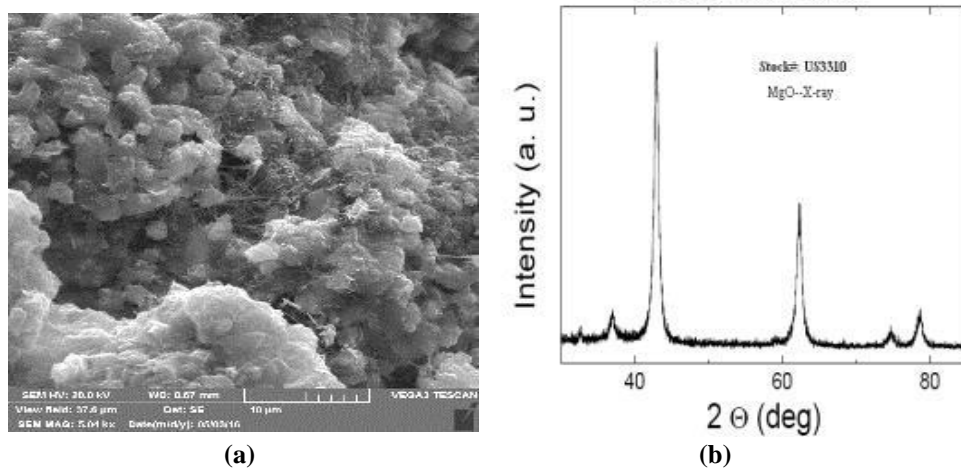


Figure 2: (a) SEM plate and (b) XRD patterns of the MgO NPs

3.2. Effect of pH

The pH is an important parameter on adsorption processes. The effect of different pH (in the range 3-11) on the adsorption of RB19 at the contact time of 60 min is shown in Figure 3. The results show that at pH 3, RB19 removal was increased. The RB19 is anionic and the MgO NPs pH_{ZPC} obtained was 12.4. At pH less than pH_{ZPC} , the catalyst had a positive charge. In acidic pH, electrostatic adsorption between RB19 negative ions and positively charged catalyst increased, therefore, the increase in efficiency of removal [6, 32]. From pH 7-11, the concentration of OH^- ions increased, therefore, competition between them and the anions increased. The efficiency of removal decreased because of the repulsive force between the negative charged catalyst and RB19 anions [6, 33].

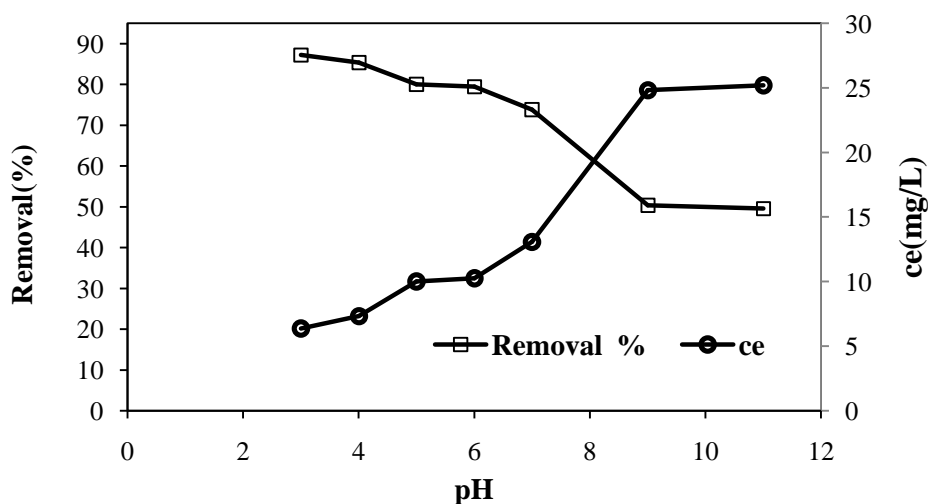


Figure 3: Effect of pH on percentage removal of RB19
(Time: 60 min, dosage: 0.9 g/L, RB19 concentration: 50 mg/L)



3.3. Effect of adsorbent dosage

The effect of adsorbent dosage on the removal of RB19 was studied by varying the dosage of adsorbent from 0.3 to 2.3 g/L at optimum pH (3) and dye concentration 50 mg/L. From Figure 4, it is evident that the dosage of adsorbent significantly influences the amount of RB19 adsorbed. The percentage of RB19 removal steeply increased with the adsorbent loading up to 1.5g/L. Increasing the MgO NPs resulted to more production of hydroxyl radicals because of the increase in the active adsorption sites and free electrons in the conductive bond, so an increase in efficiency of removal [34, 35].

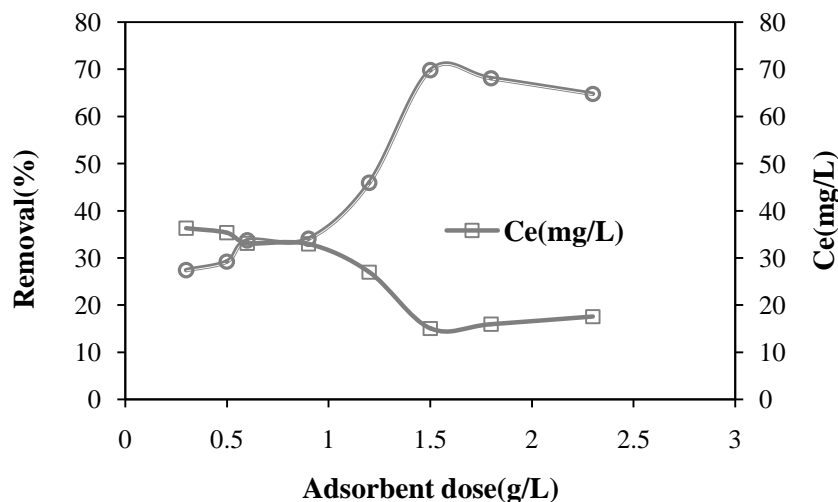


Figure 4: Effect of adsorbent dosage on percentage removal of RB19
(Time: 60 min, pH: 3, dye concentration: 50mg/L).

3.4. Effect of initial concentration

To determine the effect of initial RB19 concentration on the adsorption process, the initial concentration of RB19 was varied from 50 to 150 mg/L at the optimum pH 3, adsorbent dosage of 1.5g/L and contact time of 60 min. As presented in Fig.5, the maximum efficiency was achieved at an initial RB19 concentration of 90 mg/L. The RB19 removal efficiency on MgO NPs was increased from 58.16% to 79% by increasing the initial concentration of RB19 from 50 to 90 mg/L and it is decreased from 79% to 78.43% removal efficiency. The results showed that the effect of initial RB19 concentration reduced the removal efficiency when the concentration was increased. It is because of the limited adsorption sites which will be saturated more quickly and thus the reduction in removal efficiency [36].

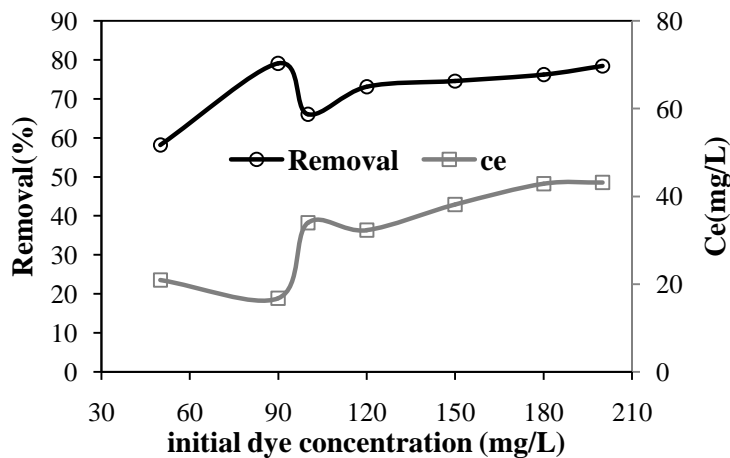


Figure 5: Effect of RB19 concentration on percentage removal of RB19
(Time: 60 min, dosage: 1.5g/L, pH: 3)



3.5. Effect of contact time and temperature

Figure 6 shows the effect of contact time (20, 40, 60, 80, 120, 150 min) and solution temperature (293, 313, 308 K) on the percentage removal efficiency of RB19 on MgO NPs at constant initial RB19 concentration of 90 mg/L and optimum adsorbent dosage of 1.5 g/L and optimum pH 3. By increasing the contact time, the efficiency of RB19 depletion was increased. The rapid increase in the depletion efficiency at the early time is that by passing time, the made cavity and corrosion on MgO NPs level will be expanded and so the increase in the cross-section of adsorption efficiency [20, 21] is consistent with other studies [20].

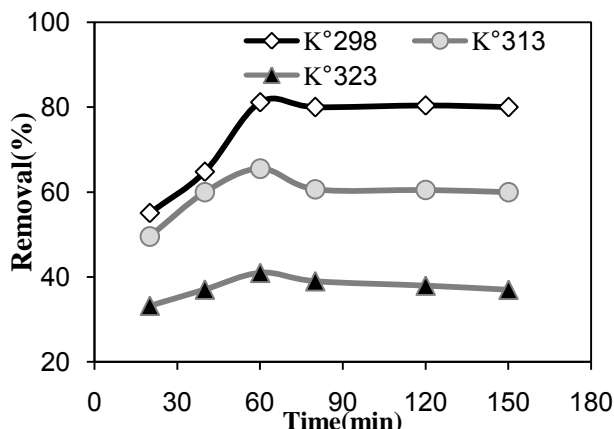


Figure 6: Effect of contact time on percentage removal of RB19 (RB19 concentration: 90 mg/L, dosage: 1.5g/L, pH: 3)

3.6. Adsorption Kinetics

The kinetic parameters and correlation coefficients (R^2) for each kinetic model are presented in Table 1. The R^2 of the pseudo first second-order model was low (0.8206, 0.7858 and 0.7639 at 298, 313 and 323 K respectively) which depicts low correlation with the RB19 adsorption process. The pseudo-second-order model showed suitable correlation for RB19 absorption on MgO NPs. The R^2 of kinetic models suggested that the pseudo-second-order model mechanism is predominant which means the uptake process follows the pseudo-second-order kinetic model expression with R^2 of 0.9949, 0.9828 and 0.9829 at 298, 313 and 323 K respectively, which proposes a chemisorption process [10].

Table 1: The adsorption kinetic model constants for the removal of RB19

Temperature (K)	Pseudo-second-order			Pseudo-first-order		R^2
	K_2	q_e	R^2	K_L	q_e	
298	0.003	49.26	0.9949	0.025	16.62	0.8206
313	0.100	34.24	0.9828	0.004	6.720	0.7858
323	0.007	22.62	0.9829	0.005	11.24	0.7639

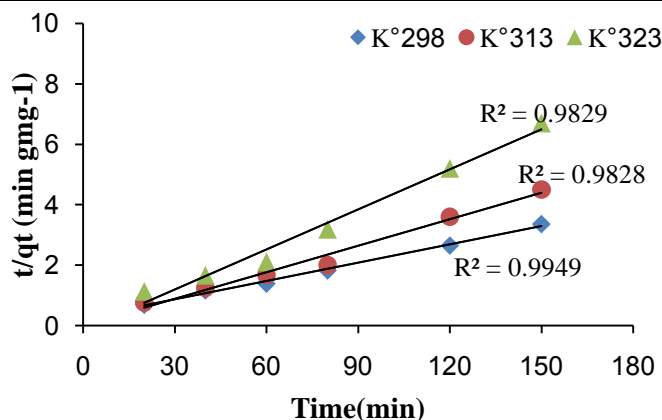


Figure 7: Pseudo-second-order model plot of RB19 adsorption on MgO NPs



3.7. Adsorption Isotherm

The compliance of the Freundlich, Langmuir and Temkin models with the equilibrium experimental results studied. The correlation coefficient of the Freundlich isotherm model was higher than other models ($R^2 = 0.924$). This implies that the equilibrium adsorption data complied with the Freundlich isotherm model. Also, the intensity of adsorption, n -value (0.35) lies within 1-10 revealing the favourability of the RB19 adsorption process [28].

Table 2: The adsorption isotherms constants for the removal of RB19 on MgO NPs

Langmuir isotherm			Freundlich isotherm			Temkin isotherm			
K_L	q_m	R_L	R^2	K_f	n	R^2	B_T	A_T	R^2
0.02	7.9	0.3	0.604	0.002	0.35	0.924	73.6	2.8	0.864

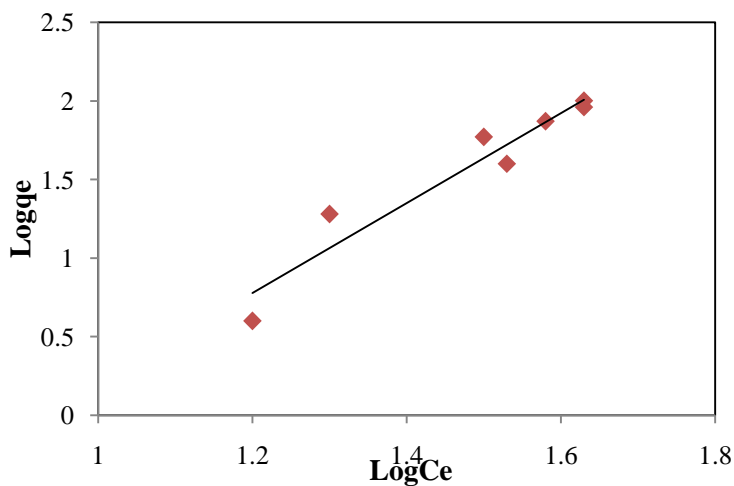


Figure 8: Freundlich model plot of RB19 adsorption on MgO NPs

3.8. Thermodynamic study

The three thermodynamic parameters of RB19 adsorption on MgO NPs are shown in Table 2. ΔH^0 was found to be 6.332 KJ/mol. ΔG^0 values were obtained as 12.29, 12.59, 12.79 KJ/mol temperatures at temperatures of 298, 313, 323K, respectively. The positive value of ΔH^0 and state that the process of RB19 adsorption is endothermic, respectively. Positive small values of free energy indicate a non-spontaneous process of the biosorption which could be promoted by performing the adsorption process at controlled temperature [37, 38]. Also, the negative value of ΔS^0 was caused by the decrease in the efficiency of the reaction to a higher temperature [36].

Table 3: Thermodynamic parameters for the adsorption of RB19

Temperature (K)	ΔG^0 (KJ/mol)	ΔH^0 (KJ/mol)	ΔS^0 (KJ/molK)
298	12.29		
313	12.59	6.332	-0.02
323	12.79		

4. Conclusion

In this study, the ability of magnesium oxide nanoparticles (MgO NPs) on reactive blue 19 (RB19) adsorption efficiency was studied and the impacts of the process parameters that is, contact time, pH, adsorbent dosage and initial RB19 concentration were investigated. It has been observed that the adsorbent was able to remove the RB19 efficiently. The maximum removal efficiency at the optimum conditions (time = 60min, pH = 3, dosage = 1.5g/L) was found to be 81% for MgO NPs. The Freundlich adsorption isotherm and the pseudo-second-order kinetic models best described the



removal of RB19 on MgO NPs. RB19 adsorption on MgO NPs was found to be endothermic in nature. The negative ΔS^0 and positive ΔG^0 was caused by the decrease in the efficiency of the reaction to higher temperature. Conclusively, this method can be used as for treatment of - contaminated wastewaters.

5. Conflict of Interest

There is no conflict of interest associated with this work.

References

1. Holkar, C.R., Jadhav, A.J., Pinjari, D.V., Mahamuni, N.M. and Pandit, A.B. (2016). A critical review on textile wastewater treatments: possible approaches. *Journal of Environmental Management* 182, pp. 351-366.
2. Rietschel, R.L, Fowler, J.F. and Fisher, A.A. (2008). Fisher's contact dermatitis in textiles and shoes. BC Decker Inc, Ontario, pp. 339-401.
3. Daneshvar, N., Salari, D. and Khataee, A.R. (2004). Photo catalytic degradation of azo dye acid red 14 in water on ZnO as an alternative catalyst to TiO₂. *J Photochemistry and Photobiology A: Chemistry* 162 (2-3), pp. 317-322.
4. Cheng, M.Y., Yu, I.C. and Wang, P.K. (2002). Degradation of azo dye Procion Red MX-5B by photo catalytic oxidation. *Chemosphere* 46(6), pp. 905-912.
5. Hachem, C., Bocquillon, F., Zahraa, O. and Bouchy, M. (2001). Decolorisation of textile industry wastewater by the photo catalytic degradation process. *Dyes and Pigments* 49(2), pp. 117-125.
6. El-Bindary, A.A., Abd El-Kawi, M.A., Hafez, A.M., Rashed, I.G.A and Aboelnaga, E.E. (2016). Removal of reactive blue 19 from aqueous solution using rice straw fly ash. *Journal of Materials and Environmental Science* 7 (3), pp. 1023-1036.
7. Rajkumar, D., Song, B.J. and Kim, J.G. (2007). Electrochemical degradation of Reactive Blue 19 in chloride medium for the treatment of textile dyeing wastewater with identification of intermediate compounds. *Dyes and Pigments* 71, pp. 935-944.
8. Ahmadi, Sh. and Kord Mostafapour, F. (2017). Treatment of Textile wastewater using a combined coagulation and DAF processes, Iran, 2016. *Archives of Hygiene Sciences* 6(3), pp. 229-234.
9. Lee, J.W., Choi, S.P., Thiruvengatchari, R., Shim, W.G. and Moon, H. (2006). Evaluation of the performance of adsorption and coagulation processes for the maximum removal of reactive dyes. *Dyes and Pigments* 69, pp. 196-203.
10. Igwegbe, C. A., Onukwuli, O. D. and Nwabanne, J. T. (2016). Adsorptive removal of vat yellow 4 on activated *Mucuna pruriens* (velvet bean) seed shells carbon. *Asian Journal of Chemical Sciences* 1(1), pp. 1-16.
11. Gupta, V.K., Ali, I. and Vipin, K. (2007). Adsorption studies on the removal of Vertigo Blue 49 and Orange DNA13 from aqueous solutions using carbon slurry developed from a waste material. *Journal of Colloid Interface Science* 315, pp. 87-96.
12. Ozmihci, S. and Kargi, F. (2006). Utilization of powdered waste sludge (PWS) for removal of textile dyestuffs from wastewater by adsorption. *Journal of Environmental Management* 81, pp. 307-14.
13. Rahdar S., Igwegbe C.A., Rahdar A., Ahmadi S., Efficiency of sono-nano-catalytic process of magnesium oxide nanoparticle in removal of penicillin G from aqueous solution. *Desal. Wat. Treat.* 106 (2018)330-335. doi:10.5004/dwt.2018.22102
14. Aos Santos, AB., Cervantes, F.J. and van Lier, J.B. (2007). Review paper on current technologies for decolorisation of textile wastewaters: perspectives for anaerobic biotechnology. *Bioresource Technology* 98, pp. 2369-2385.
15. Jiantuan, G.E. and Jihui, Q.U. (2004). Ultrasonic irradiation enhanced degradation of azo dye on MnO₂. *Applied Catalysis B: Environmental* 47, pp. 133-140.



16. Khoshnamvand, N, Ahmadi S, Mostafapour FK, Kinetic and isotherm studies on ciprofloxacin an adsorption using magnesium oxide nanoparticles. *J App Pharm Sci*, 2017; 7(11): 079-083.
17. Raizada, P., Singh, P., Kumar, A., Pare, B. and Jonnalagadda, SB. (2014). Zero valent iron-brick grain nanocomposite for enhanced solar-Fenton removal of malachite green. *Separation and Purification Technology* 133, pp. 429-3.
18. Yahya, S., Al-Degs, M.I., El-Barghouthi, A.H., Sheikh, El. and Walker, G.M. (2008). Effect of solution pH, ionic strength, and temperature on adsorption behavior of reactive dyes on activated carbon. *Dyes and Pigments* 77, pp. 16-23.
19. Tajbakhsh, M., Farhang, M., Hosseini, A. (2014). MgO nanoparticles as an efficient and reusable catalyst for aza-Michael reaction. *Journal of the Iranian Chemical Society* 11(3), pp. 665-72.
20. Kermani, M., Bahrami Asl, F., Farzadkia, M., Esrafil, A., Salahshur Arian, S., Arfaeinia H, et al. (2013). Degradation efficiency and kinetic study of metronidazole by catalytic ozonation process in presence of MgO nanoparticles. *Urmia Medical Journal* 24(10), pp. 839-50.
21. Nga, N.K., Hong, P.T.T., Lam, T.D. and Huy, T.Q. (2013). A facile synthesis of nanostructured magnesium oxide particles for enhanced adsorption performance in reactive blue 19 removal. *Journal of Colloid and Interface Science* 398, pp. 210-6.
22. Mohammadi, A. S., Sardar, M., Mohammadi, A., Azimi, F. and Nurieh, N. (2013). *Archives of Hygiene Sciences* 2(4), pp. 158-164.
23. Ahmadi, Sh. and Kord Mostafapour, F. (2017). Tea waste as a low-cost adsorbent for the removal of COD from landfill leachate: kinetic study. *Journal of Scientific and Engineering Research* 4 (6), pp. 103-108.
24. Igwegbe, C.A., Onyechi, P.C. and Onukwuli, O.D. (2015) Kinetic, isotherm and thermodynamic modelling on the adsorptive removal of malachite green on *Dacryodes edulis* seeds. *Journal of Scientific and Engineering Research*, 2015, 2(2), pp. 23-39.
25. Bulut, Y., Gözübenli, N. and Aydin, H. (2007). Equilibrium and kinetics studies for adsorption of direct blue 71 from aqueous solution by wheat shells. *Journal of Hazardous Materials* 144(1-2), pp. 300-306.
26. Rahdar, S. and Ahmadi, Sh. (2016). Removal of phenol and aniline from aqueous solutions by using adsorption onto *Pistacia terebinthus*: study of adsorption isotherm and kinetics. *Journal of Health Research in Community* 2, 35-45.
27. Igwegbe, C.A., Onyechi, P.C., Onukwuli, O.D. and Nwokedi, I.C. (2016) Adsorptive treatment of textile wastewater using activated carbon produced from *Mucuna pruriens* seed shells. *World Journal of Engineering and Technology*, 4, pp. 21-37.
28. Menkiti, M. C., Okoani, A. O. and Ejimofor, M. I. (2018). Adsorptive study of coagulation treatment of paint wastewater using novel *Brachystegia eurycoma* extract, *Applied Water Science* 8, 189. <https://doi.org/10.1007/s13201-018-0836-1>
29. Zazouli, M.A., Balarak, D., Karimzadeh, F., and Khosravi, F. (2014). Removal of fluoride from aqueous solution by using of adsorption onto modified Lemna Minor: adsorption isotherm and kinetics study. *Journal of Mazandaran University Medical Science* 24(109), pp. 41-8.
30. Balarak, B. (2016). Kinetics, isotherm and thermodynamics studies on bisphenol A adsorption using barley husk. *International Journal of ChemTech Research* 9(5), pp. 681-690.
31. Okeola, O.F., Odeunmi, E.O. and Ameen, O.M. (2012). Comparison of sorption capacity and surface area of activated carbon prepared from *Jatropha curcas* fruit pericarp and seed coat. *Bulletin of the Chemical Society of Ethiopia* 26(2), pp. 171-180.
32. Nasir, A., Khan, M., Siddique, M., Wahid, F. and Khan, R. (2015). Removal of reactive blue 19 dyes by sono, photo and sonophotocatalytic oxidation using visible light. *Ultrasonics Sonochemistry* 26, pp. 370–377.
33. Kord Mostafapoor, F., Ahmadi, Sh., Balarak, D. and Rahdar, S. (2017). Comparison of dissolved air flotation process for aniline and penicillin G removal from aqueous solutions. *Hamedan University of Medical Sciences* 23(4), pp. 360-369.



34. Samadi, M.T., Kashitarash Esfahani, Z., Ahangari, F., Ahmadi, Sh. and Jafari, J. (2013). Nickel removal from aqueous environments using carbon nanotubes. *Water and Wastewater* 24, pp. 38–44.
35. Bazrafshan, E. and Ahmadi, Sh. (2017). Removal COD of landfill leachate using coagulation and activated tea waste (ZnCLR2R) adsorption. *International Journal of Innovative Science, Engineering & Technology* 4(4), pp. 339-347.
36. Manivannan, P., Arivoli, S. and Mohammed, R. (2015). Equilibrium and thermodynamics studies on the removal of iron (III) onto activated Hibiscus Sabdariffa stem nano carbon. *International Journal of ChemTech Research* 8(10), pp. 346-354.
37. Nagy, B., Mănzatu, C., Măicăneanu, A., Indolean, C., Lucian, B.-T. and Majdik, C. (2017). Linear and nonlinear regression analysis for heavy metals removal using *Agaricus bisporus* macrofungus, *Arabian Journal of Chemistry* 10, S3569–S3579.
38. Schneider, R.M., Cavalin, C.F., Barros, M.A.S.D., Taveres, C.R.G., 2007. Adsorption of chromium ions in activated carbon. *Chem. Eng. J.* 132, 355.

